Author/s:
Farrugia, BL;Mi, Y;Kim, HN;Whitelock, JM;Baker, SM;Wiesmann, WP;Li, Z;Maitz, P;Lord, MS

Title:
Chitosan-Based Heparan Sulfate Mimetics Promote Epidermal Formation in a Human Organotypic Skin Model

Date:
2018-09-05

Citation:
Farrugia, B. L., Mi, Y., Kim, H. N., Whitelock, J. M., Baker, S. M., Wiesmann, W. P., Li, Z., Maitz, P. & Lord, M. S. (2018). Chitosan-Based Heparan Sulfate Mimetics Promote Epidermal Formation in a Human Organotypic Skin Model. Advanced Functional Materials, 28 (36), https://doi.org/10.1002/adfm.201802818.

DOI: 10.1002/ ((please add manuscript number))

Article type: (**Full Paper**)

Chitosan-based heparan sulfate mimetics promote epidermal formation in a human organotypic skin model

Brooke L. Farrugia, Yaolei Mi, Ha Na Kim, John M. Whitelock, Shenda Baker, William P. Wiesmann, Zhe Li, Peter Maitz, Megan S. Lord*

Dr B. L. Farrugia, Y. Mi, H.N. Kim, Prof. J. M. Whitelock, A/Prof. M. S. Lord

Graduate School of Biomedical Engineering, UNSW Sydney, Sydney NSW 2052, Australia.

Email: b.farrugia@unsw.edu.au

Dr S. Baker, Dr W. P. Wiesmann

Synedgen Inc, Claremont, CA, USA

Dr Z. Li, Prof. P. Maitz

Burns Unit, Concord Repatriation General Hospital, Concord, NSW 2130, Australia

Sydney Medical School, University of Sydney, Sydney, NSW 2006, Australia

Keywords: chitosan; heparan sulfate; fibroblast growth factor; skin wound healing.

Biomimetic materials that replicate biological functions have great promise for use as therapeutics in regenerative medicine applications. Heparan sulfate (HS) is the natural binding partner for growth factors enabling longer half-lives and potentiation of their signaling. In this study a water soluble chitosan-arginine was modified with sulfate moieties in order to mimic the structure of HS. Sulfated chitosan-arginine with a degree of sulfation of 58% bound fibroblast growth factor 2 with higher affinity than HS. The sulfated chitosan-arginine also promoted epithelial cell migration and supported the formation of an expanded epidermis in an organotypic skin model. Furthermore, sulfated chitosan-arginine promoted the expression of the HS proteoglycan, perlecan, by both epithelial and fibroblast cells. Perlecan itself modulates the activity of mitogens and is essential for the formation of the epidermis. The synthesized sulfated Ch-Arg derivatives mimicked HS, supported formation of the epidermis and thus have the potential to assist in wound healing.

1. Introduction

The use of biomimetic materials for tissue engineering and regenerative applications holds great potential due to their ability to mimic the functional properties of biological molecules. Growth factors are signaling molecules that regulate events in tissue development and repair including cell proliferation, differentiation and migration.[1, 2] Thus, molecules or materials that bind to and potentiate the activity of growth factors are promising for tissue engineering and drug delivery applications.

Many growth factors naturally bind to and are both protected and potentiated by heparan sulfate (HS) chains that decorate proteoglycans present in the extracellular matrix (ECM) and on the cell surface [3, 4]. These growth factors are described as heparin-binding as heparin is often used as a model for HS due to its availability from the pharmaceutical market.[5] While heparin expression is restricted to mast cell subsets,[6] HS is widely distributed throughout the body and is thus the natural binding partner for heparin-binding growth factors.[4] Heparin and HS are structurally similar linear polysaccharides composed of repeating disaccharide units of uronic acid and glucosamine.[4] The residues can be sulfated at positions 2-O and N on the uronic acid residues as well as the 3-O and 6-O positions on the glucosamine residues to produce HS/heparin substituted with sulfate groups in the range of 0-55% [7, 8]. Growth factors bind to sulfated domains within HS/heparin chains, thus the density as well as overall level of sulfation are important for the fine tuning of growth factor binding and signaling.[9, 10] The low abundance of HS isolated from tissues limits its biomedical application, hence the development of HS/heparin mimetics will enable the use of materials that potentiate growth factors required for tissue engineering.

Heparin binding growth factors are essential for skin development and repair and include members of the fibroblast growth factor (FGF) family, FGF1, FGF2, FGF4, FGF7 (also known as keratinocyte growth factor) and FGF10, platelet derived growth factor and epidermal growth factor with roles in cell proliferation and migration.[1, 11, 12] These growth factors have been explored for skin repair alone or incorporated into various scaffolds that control their release via properties such as porosity, pH or protease activity.[5] These approaches can extend the half-life of growth factors, however not to the extent of heparin/HS *in vivo*, and their therapeutic use often require supra physiological concentrations, resulting in undesired side effects.[13] Thus the development of HS mimetics for both

de novo synthesized growth factor protection and activity as well as growth factor delivery is of interest for therapeutic applications.

HS/heparin mimetics have been synthesized using a number of different techniques including chemical synthesis, chemoenzymatic synthesis and chemical modification of polysaccharides.[14] Most of these approaches have focused on heparin mimetics for anticoagulant activity, while some have also reported the synthesis of HS mimetics such as oligosaccharides based on D-glucosamine that bind FGF2 and vascular endothelial growth factor (VEGF)165.[15] Chemical approaches have not yet yielded structures larger than octasaccharides while chemoenzymatic synthesis has produced oligosaccharides up to decasccharides.[16] Chemical modification of polysaccharides enables the production of longer HS mimetics up to 8,000 saccharides in length such as for sulfated hyaluronan enabling a much larger size range than chemical approaches to optimise biological activity.[14] Chitosan, a polyglucosamine derivative of chitin, has a similar polymer structure to heparin/HS, but without sulfate moieties. Chitosan is an attractive polysaccharide to modify with sulfates as it also possesses properties widely acknowledged to be of benefit in wound healing, most notably its anti-bacterial propoerties and biodegradability.[17, 18] While chitosan has been used as a hemostatic agent in biomedical applications,[17] the modification of chitosan to incorporate sulfate groups has generated interest due to its anticoagulant properties.[19, 20] Sulfated derivatives of chitosan also demonstrate the ability to bind FGF2,[21] VEGF165,[22] EGF[23] and bone morphogenic protein (BMP)2,[24, 25] depending on the position of substitution with sulfate. However, the limited solubility of chitosan at physiological pH is a disadvantage for its therapeutic application. Peptide modified chitosan, such as chitosan-arginine, however, is water soluble at physiological pH and maintains its antimicrobial activity.[26, 27]

The derivatization of chitosan with arginine has been reported by our group with single amino acids (Ch-Arg) via protection of the function group.[26] Other groups use an unprotected functional group to yield chitosan modified with poly(arginine chains).[28, 29] Poly(arginine) exhibits cell penetrating functions and thus may direct the site of activity of the material such as reported for chitosan-histidine-arginine for gene delivery, while single amino acids display much reduced cell penetrating properties.[29, 30] Sulfate derivatized Ch-Arg binds and signals FGF2[31] indicating that it may have a positive effect on wound healing. Addditionally, electrospun chitosan-poly(arginine) enhanced wound closure in a rat full thickness wound model[32] while EGF bound to sulfated chitosan/PLGA composite nanofibers promoted re-epithelialization in a mouse full thickness wound model.[23]

The aims of this study were to functionalize Ch-Arg with sulfate groups to mimic the structure of HS and to explore their potential to support skin wound healing in terms growth factor binding, epithelial cell migration and the formation of dermal and epidermal tissue in an organotypic skin model.

2. Results

2.1 Characterization of chitosan-based HS mimetics

The modification of Ch-Arg with sulfate groups was performed in order to mimic the structure of HS with sulfate residues in the substitution range of 0-55% that bind and potentiate the signaling of growth factors. The sulfation method employed can modify positions C_2, C_3 or C_6 on the chitosan backbone and C_8 or C_{12} on the arginine side

chain **(Figure 1A)**. The ability to control the extent of sulfate modification of Ch-Arg was explored by varying the amount of sulfating agent added to the reaction, either in excess (6× equiv) or limited (0.5× equiv). Elemental analysis confirmed that this approach yielded a low level of sulfur modification of 0.78% when the sulfating agent was limited, referred to herein as LS-Ch-Arg **(Table 1)**. Additionally, when the sulfating agent was used in excess there was a higher level of sulfur modification of Ch-Arg of 8.04%, referred to herein as HiS-Ch-Arg **(Table 1)**. Calculation of the degree of sulfation indicated that LS-Ch-Arg and HiS-Ch-Arg were 3 and 58% sulfated, respectively **(Table 1),** that mimicked HS with a low and high level of sulfate modification, respectively. ATR-FTIR confirmed the incorporation of sulfate into these materials by the appearance of peaks characteristic of S=O and C-O-S bonds at 1250 and 800cm^{-1}, respectively, that were absent in Ch-Arg **(Figure 1B)**. Zeta potential measurements indicated that LS-Ch-Arg was slightly less positively charged than Ch-Arg while HiS-Ch-Arg was significantly ($p \leq 0.001$) less positively charged than Ch-Arg and had an overall negative charge **(Figure 1C)**. This reduction in positive charge is attributed to the negative charge imparted by the incorporated sulfate groups.

The HSQC spectra from 2D NMR were used to determine the position of sulfation. Peak shifts were observed in the ^{1}H signal assigned to GlcNAc H_2, H_3 and GlcN H_3 in LS-Ch-Arg indicating modification of these residues compared to Ch-Arg (**Figure**

1D). Peak shifts were observed for HiS-Ch-Arg compared to Ch-Arg at the C_2, C_3, C_6, and C_8 positions (y-axis) and H_2, H_3 (GlcNAc), and H_3 (GlN) positions (x-axis), confirming sulfate modification of both the chitosan backbone and the arginine side chain of HiS-Ch-Arg **(Figure 1E)**. Together these data confirmed that Ch-Arg was modified with sulfate at positions similar to those present in HS with LS-Ch-Arg resembling HS with a low level of sulfate modification and HiS-Ch-Arg resembling HS with a high level of sulfate modification.

2.2 Chitosan-based HS mimetics are not cytotoxic

Ch-Arg and the sulfated derivatives were evaluated for their cytotoxicity using keratinocytes and fibroblasts over an exposure period of 72 h. Neither Ch-Arg nor the sulfated derivatives when used at 10 μg mL^{-1} significantly affected cell number over the analysis period compared to cells grown in basal medium **(Figure 2A and B)**. Thus this concentration was used for subsequent cell-based experiments.

2.3 Chitosan-based HS mimetics promote HS proteoglycan expression

The HS proteoglycans secreted by both dermal fibroblasts and keratinocytes cultured in basal medium were analyzed by mass spectrometry and found to include ECM, perlecan, agrin and collagen type XVIII, and cell surface, glypicans and syndecan-4, molecules **(Table 2)**. In addition,

keratinocytes secreted syndecan-1, a cell surface HS proteoglycan. The MOWSE score indicates the abundance of each molecule and revealed that perlecan and agrin were the most abundant HS proteoglycans produced by fibroblasts and keratinocytes, respectively. Perlecan was the second most abundant HS proteoglycan produced by keratinocytes while only low levels of agrin were expressed by fibroblasts.

The expression of perlecan by both cell types was confirmed by immunocytochemistry and found to be cell associated for keratinocytes whereas fibroblasts produced perlecan as extracellular fibers **(Figure 3A and 3B)**. The secretion of perlecan by both cell types was confirmed by ELISA **(Figure 3C)**. Both cell types were also found to secrete HS **(Figure 3D)**. Perlecan produced by both cell types was predominantly a proteoglycan form decorated with HS as removal of the HS resulted in a major immunoreactive band at the full length protein core of approximately 460 kDa (**Figure 3E and 3F**). Fibroblast-derived perlecan exhibited a major immunoreactive band in the undigested sample in the 300 – 350kDa range, however when HS was removed the heterogeneous immunoreactive band ran at a similar molecular weight as keratinocyte perlecan without HS. This suggested that the fibroblast form of perlecan in the undigested sample may have been present in large HS-dependent aggregates that didn't enter the gel. In addition to the full length perlecan protein core, each cell type produced low abundance perlecan species in the molecular weight range 300 – 350 kDa in the undigested sample.

The ability of Ch-Arg and the sulfated derivatives to modulate perlecan gene (*HSPG2*) expression was assessed by qPCR. Short term exposure (4h) of both keratinocytes and fibroblasts to either LS-Ch-Arg or HiS-Ch-Arg upregulated *HSPG2* expression compared to cells grown in basal medium **(Figure 4A and 4B)**. In contrast, exposure of these cells to Ch-Arg for 4 h downregulated *HSPG2* expression

(Figure 4A and 4B). Longer term exposure (24h) of keratinocytes to either Ch-Arg or LS-Ch-Arg downregulated *HSPG2* expression compared to cells grown in basal medium, while HiS-Ch-Arg had no effect **(Figure 4A)**. Similarly, longer term exposure (24h) of fibroblasts to either Ch-Arg or the sulfated derivatives had no effect on *HSPG2* expression compared to cells grown in basal medium **(Figure 4A)**. Together these data suggest that the chitosan-based HS mimetics can modulate perlecan expression in the initial period following exposure.

2.4 Chitosan-based HS mimetics have a high affinity for FGF2, but not FGF7

HS binds a wide range of growth factors. Ch-Arg and the sulfated derivatives were evaluated for their ability to bind selected growth factors involved in skin wound healing, FGF2 and FGF7. FGF2 and FGF7 are heparin binding growth factors, thus their level of binding to the Ch-Arg preparations was compared to the HS chains on perlecan, a major component of basement membranes and involved in FGF binding and signaling.[10, 33] FGF7 also binds to the protein core of perlecan,[34] thus perlecan in the absence of its HS chains was also used as a positive control. Immunopurification of perlecan produced by both keratinocytes and fibroblasts yielded amounts that were too low to be used to analyze growth factor interactions (data not shown). Thus the well-characterized endothelial derived perlecan that is exclusively decorated with HS[35] was used as a model for both keratinocyte and fibroblast derived perlecan.

Analysis of the level of binding of FGF2 to Ch-Arg and its sulfated derivatives indicated that HiS-Ch-Arg bound significantly (p<0.05) more FGF2 than either Ch-Arg or LS-Ch-Arg **(Figure 5A and Supplementary Figure 1B)**. The HS chains on perlecan bound FGF2 while their removal (denoted

Perlecan-HS) significantly reduced the level of binding suggesting that FGF2 bound to perlecan via its HS chains (p<0.05). Interestingly, HiS-Ch-Arg supported the same level of FGF2 binding as the HS chains on perlecan **(Figure 5A)**, suggesting that HiS-Ch-Arg could mimic the FGF2 binding possessed by perlecan HS chains. Measurement of the binding kinetics between FGF2 and HiS-Ch-Arg indicated both rapid association and dissociation rates **(Figure 5B)**. These binding curves were modelled as Langmuir binding, which assumes 1:1 interactions, and established that the association (k_a) and dissociation rates (k_d) were 160 $M^{-1}s^{-1}$ and 1 × 10^{-3} s^{-1}, respectively. Similarly the binding between FGF2 and perlecan exhibited rapid association and dissociation rates with a lower level of interaction compared to HiS-Ch-Arg **(Figures 5B and 5C)**. Modelling of the binding between FGF2 and perlecan indicated that the association and dissociation rates were 102 $M^{-1}s^{-1}$ and 1.8 × 10^{-3} s^{-1}, respectively. The equilibrium dissociation constant (K_D) of FGF2 for HiS-Ch-Arg and perlecan were found to be 6.4 µM and 1.74 µM, respectively, indicating that FGF2 had a higher affinity for HiS-Ch-Arg than the perlecan HS chains. Additionally, the χ^2 values from the model for both HiS-Ch-Arg and perlecan were both greater than 2 indicating that FGF2 bound to each of these molecules via multivalent interactions.

FGF7 bound to Ch-Arg and the sulfated derivatives at low levels with no significant difference between the Ch-Arg preparations **(Figure 5D and Supplementary Figure 1C)**. Perlecan bound significantly ($p \leq 0.05$) more FGF7 than any of the Ch-Arg preparations **(Figure 5D)** and predominantly bound FGF7 via its protein core although there was a significant reduction (p<0.05) in the level of FGF7 binding to perlecan without its HS chains suggesting that the HS chains may also be involved in the binding **(Figure 5D and Supplementary Figure 1C)**. Together these results indicated that HiS-Ch-Arg mimics the FGF2 binding of HS, but has a low capacity to bind FGF7.

2.5 Chitosan-based HS mimetics promote epithelial cell migration

The effect of Ch-Arg and the sulfated derivatives on keratinocyte migration in a 'scratch assay' was explored over a 72 h period **(Figure 6A)**. Sample phase contrast images show the migration of the keratinocytes in the central region of the images over 72 h exposed to the different conditions **(Figure 6A)**. The images were analyzed by measuring the area between the two migrating cell fronts at each time point and presented as a proportion of the initial area **(Figure 6B)**. Keratinocytes exposed to serum free medium containing HiS-Ch-Arg exhibited the greatest migration with complete wound closure within 72 h. Cells exposed to HiS-Ch-Arg exhibited a significant increase (p<0.05) in migration compared to cells exposed to serum free medium alone or supplemented with Ch-Arg, LS-Ch-Arg or heparin **(Figure 6A and 6B)**. However, neither Ch-Arg, LS-Ch-Arg nor heparin promoted keratinocyte migration compared to serum free medium **(Figure 6A and 6B)**. As FGF2, but not FGF7, bound to HiS-Ch-Arg (**Figure 5**), an anti-FGF2 antibody was trialed in the keratinocyte migration assay. FGF2 is a mitogenic growth factor and the inhibition of its activity with a function blocking antibody had no effect on the level of keratinocyte migration (**Supplementary Figure 2**) suggesting that cell proliferation did not play a major role in the observed keratinocyte migration. Together these data suggest that mitogenic signals acting on keratinocytes were potentiated by HiS-Ch-Arg.

2.6 Chitosan-based HS mimetics support extracellular matrix formation in an organotypic model

In order to further explore the ability of the chitosan-based HS mimetics to support skin tissue formation, an organotypic skin model was employed. The organotypic skin model was comprised of a collagen matrix seeded with dermal fibroblasts to form the dermal component onto which keratinocytes were seeded and formed a stratified epidermis as shown by hematoxylin and eosin staining **(Figure 7A)**. The thickness of the epidermis significantly (p<0.05) increased when the model was cultured in the presence of either Ch-Arg or its sulfated derivatives compared to basal conditions **(Figure 7B)**. Additionally, the thickness of the two base layers of the epidermis, the stratum basale and the stratum spinosum, significantly (p<0.05) increased when the model was cultured in the presence of Ch-Arg compared to basal medium, however there was no difference when cultured in the presence of either of the sulfated derivatives **(Figure 7C)**.

In order to establish that this model was representative of skin, it was probed for the expression and localization of basement membrane components, laminin and collagen type IV. Laminin was expressed both intracellularly and extracellularly by keratinocytes in the epidermis as well as intracellularly by fibroblasts in the dermis **(Figure 8A)**. The staining pattern in the epidermis displayed a gradient from intense

staining in the basal layer to less intense staining in the upper layers of denucleated keratinocytes **(Figure 8A)**. Treatment of the model with Ch-Arg and the sulfated derivatives did not alter the localization of laminin, however the expanded epidermis in each of these conditions resulted in an expanded zone of laminin deposition surrounding the denucleated keratinocytes **(Figure 8A)**. Additionally, the expanded stratum basale and the stratum spinosum in the models treated with Ch-Arg exhibited an expanded zone of laminin expression **(Figure 8A)**. Collagen type IV was present in the collagen-based dermis as detected by staining throughout this region **(Figure 8B)**. Additionally, keratinocytes in the basal layer at the epidermal-dermal junction produced collagen type IV (**Figure 8B**, arrows). Treatment of the model with HiS-Ch-Arg resulted in intracellular expression of collagen type IV by the basal keratinocytes, while no other treatment altered collagen type IV expression compared to the basal condition **(Figure 8B)**. Together the distribution of laminin and collagen type IV indicated that the model expressed basement membrane components at their expected locations. Additionally, these data demonstrate that the addition of Ch-Arg supported an expanded epidermis that expressed both laminin and collagen type IV throughout this region.

Sulfated Ch-Arg derivatives were able to promote perlecan expression at early time points in cultures of both keratinocytes and fibroblasts **(Figure 4)**, thus it was of interest to establish whether these treatments could affect perlecan localization in the

organotypic model. Perlecan was located intracellularly within keratinocytes in the basal layer as well in the upper layers of denucleated keratinocytes **(Figure 9A)**. Perlecan was also produced by fibroblasts located in the dermis, and localized both intracellularly and pericellularly **(Figure 9A)**. Treatment of the model with Ch-Arg and the sulfated derivatives did not alter the localization of perlecan, however the expanded epidermis in each of these conditions resulted in an expanded zone of perlecan deposition surrounding the denucleated keratinocytes as well as in both the stratum basale and the stratum spinosum **(Figure 9A)**.

Cell surface HS proteoglycans are also important for the signaling of heparin-binding growth factors, thus the distribution of synedecan-1 and -4 was investigated in the model. Syndecan-1 was located on the cell surface of basal keratinocytes, but was not found within the dermis, as was expected from the mass spectrometry results **(Figure 9B and Table 1)**. Ch-Arg and LS-Ch-Arg supported the expression of syndecan-1 throughout the expanded basal layer (**Figure 9B**). Syndecan-4 was located intracellularly in keratinocytes in the basal layer as well as in the upper layers of denucleated keratinocytes **(Figure 9C)**. Syndecan-4 was also located intracellularly in fibroblasts in the dermis **(Figure 9C)**. The expression of HS in the organotypic model was also explored as it is the principal modulator of FGF binding and signaling. HS was located on the cell surface of basal keratinocytes with diffuse staining in the upper denucleated keratinocyte layers **(Figure 9D)**. HS was also located intracellularly by

dermal fibroblasts **(Figure 9D)**. Ch-Arg and the sulfated derivatives supported the expression of HS throughout the expanded epidermis **(Figure 9D)**. Together the organotypic model revealed that Ch-Arg and the sulfated derivatives supported an expanded epidermis compared to the models cultured in basal conditions with the expression of important extracellular and cell surface molecules involved in binding and signaling FGFs for cell proliferation and tissue formation.

3. Discussion

This study demonstrated that Ch-Arg can be homogeneously modified with different levels of sulfate substitution to mimic the structure of either low or highly sulfated HS. This same starting material has been modified with a degree of sulfation up to 9% and mostly modified at the 2-N position.[31] The present study was able to achieve a higher degree of sulfation by adding the sulfating agent in excess. The modification of chitosan has been more widely explored and shown that optimization of the reaction time, temperature and pH can achieve degrees of sulfation in the range of 10 to 63%.[19, 25, 36] Thus, the extent of sulfate derivatization of Ch-Arg achieved in this study is closely aligned with that achieved for chitosan and is in the range of sulfate content of HS/heparin.[8]

Enhanced epithelial migration was demonstrated in this study in the presence of HiS-Ch-Arg in basal medium without the addition of serum or growth factors. Chitosan itself has been extensively explored for wound healing and shown to promote re-epithelialization in both normal and diabetic

rat full thickness wound models.[37] As Ch-Arg did not promote keratinocyte migration in this study at the evaluated concentration, it is likely that HiS-Ch-Arg modulated the activity of the endogenously expressed heparin-binding motogens. Interestingly, HiS-Ch-Arg did not mimic the activities of heparin in this assay suggesting differences in their sulfation density and pattern may have affected motogenic growth factor binding and signaling.[9, 10] HS/heparin binds a range of growth factors, but does not always potentiate their signaling.[35] While keratinocytes themselves do not express FGF7,[12] they produce a range of heparin binding motogens/chemokines including EGF, C-X-C motif ligand (CXCL)1 and CXCL8[38] that were likely potentiated by the presence of HiS-Ch-Arg.

This study revealed that HiS-Ch-Arg bound FGF2 with higher affinity than perlecan HS that was used as a positive control. While Ch-Arg and LS-Ch-Arg also bound FGF2, it was not at a level comparable to either HiS-Ch-Arg or perlecan HS and may be attributable to the overall positive charge of both CH-Arg and LS-Ch-Arg that did not support electrostatic binding of FGF2. This is in agreement with a previous study where sulfated Ch-Arg supported both FGF2 binding and signaling.[31] FGF2 binds to sulfated domains within HS via electrostatic interactions, thus it is likely that HiS-Ch-Arg achieved similar regions of dense sulfate modifications to support electrostatic FGF2 binding. Interestingly, Ch-Arg and the sulfated derivatives only bound low levels of FGF7 and indicated that the overall charge on these molecules had no effect on the affinity for this growth factor. Heparin oligosaccharides that differed based on

the saccharide sulfate position affected the binding to both FGF2 and FGF7[39] indicating that position of sulfate, or local charge, in addition to overall charge modulates growth factor binding. The distribution of arginine residues in FGF2 and FGF7 may account for the different level of binding to Ch-Arg and the sulfated derivatives, and perlecan. FGF2 has a higher number of arginine residues than FGF7 and the arginine residues in FGF2 are located close together providing a region of dense positive charge to bind to the negatively charged HiS-Ch-Arg and perlecan HS. The arginine residues in FGF7 are dispersed throughout the amino acid sequence and thus do not provide the same local charge as in FGF2. This study revealed that perlecan largely bound FGF7 via the protein core, in line with literature suggesting that domains III and V of perlecan support FGF7 binding.[34] This study also revealed that HS supported a low level of FGF7 binding and thus aligns with the low affinity of FGF7 for Ch-Arg and the sulfated derivatives.

Exposure of both keratinocytes and fibroblasts to the sulfated Ch-Arg derivatives upregulated *HSPG2* gene expression. Interestingly, sulfated Ch-Arg also upregulated *HSPG2* expression in chondrocytes.[31] Perlecan is a major component of the epithelial basement membrane that separates the epidermis from the dermis with well-established roles in binding and signaling mitogenic molecules.[10, 34, 35] Perlecan is essential for epidermal formation as perlecan-deficient keratinocytes form a poorly organized epidermis due to premature apoptosis and failure to stratify.[40] Thus the expanded epidermis in the organotypic model used in this study when cultured in the presence of Ch-Arg and the sulfated derivatives may be due to the upregulation of perlecan

expression. Perlecan HS-deficient (*Hspg2*$^{\Delta 3/\Delta 3}$) mice displayed delayed wound repair[41] suggesting that the HS chains are important supporting wound healing by regulating growth factor signaling, an activity ascribed to perlecan. This study also demonstrated that both keratinocyte and dermal fibroblast derived perlecan was decorated with HS, indicating the likelihood that these forms of perlecan both bind and signal growth factors required for epidermal formation. This study demonstrated that Ch-Arg and the sulfated derivatives supported HS expression in the basal layer of the epidermis. Interestingly, neither laminin nor collagen type IV, other major components of the epithelial basement membrane, deposition are affected by perlecan expression levels.[40] This is in agreement with the findings in this study where Ch-Arg and its sulfated derivatives had little effect on the expression of either laminin or collagen type IV in the organotypic model.

Cell surface HS proteoglycans syndecan-1 and -4 are also important in skin tissue formation as both syndecan-1 knock out mice display delayed wound re-epithelization[42] associated with reduced keratinocyte proliferation.[43] Additionally, syndecan-4 deficient mice display delayed wound repair.[44] These molecules were expressed throughout the basal layer in the organotypic model and colocalized with HS suggesting that they were in a position to facilitate keratinocyte migration. Together the analyses of the organotypic model suggest that the Ch-Arg and sulfated derivatives supported epidermal tissue formation with production of major components of a mature basement membrane.

4. Conclusion

This study demonstrated that Ch-Arg can be modified with a controlled level of sulfate to mimic the structure of HS with either high (58%) or low (3%) levels of sulfation. The level of sulfate

incorporated in Ch-Arg modulated its interaction with FGF2, a mitogenic heparin binding growth factor involved in epidermal tissue formation. The sulfated Ch-Arg derivatives supported epidermal tissue formation and specifically promoted perlecan expression both in isolated cultures of both keratinocytes and fibroblasts as well as in an organotypic skin model. Perlecan itself modulates the activity of mitogens and is known to be essential for the formation of the epidermis. Thus the synthesized sulfated Ch-Arg derivatives supported formation of the epidermis via both direct and indirect mechanisms. These Ch-Arg based materials may have potential as wound healing therapeutics due to their ability to bind growth factors and modulate the expression of endogenous HS proteoglycans involved in epidermal tissue formation.

5. Experimental Section

All chemicals were purchased from Sigma Aldrich (Castle Hill, Australia) unless stated otherwise.

Sulfation of chitosan-arginine: Chitosan-arginine (Ch-Arg) (85% deacetylated chitosan with single arginine amino acids constituting 24% of the total monomers on the polymer backbone; 56 kDa, purity > 99%) was synthesized by Synedgen, Inc was used as the starting material. This material was modified with varying levels of sulfation as described previously [31], with the following modifications. Dimethylformamide (30 mL) was cooled to 0 – 4 ^{o}C in an ice bath and then placed at room temperature (RT) prior to the addition of the sulfating agent, $HClSO_3$, that was added dropwise while stirring with a magnetic stirrer. The sulfating agent was either added in excess (6× equiv) or limited (0.5× equiv) to vary the level of sulfate modification. Molar equivalents were based on moles of $HClSO_3$ per *N*-acetylglucosamine unit within the chitosan backbone. The DMF·SO_3 solution was stirred until it reached RT. Ch-Arg (1 g) was dissolved in formic acid (20 mL) for 3 h at RT. DMF

(156 mL) was then added to the mixture and stirred with a magnetic stirrer for an additional 2 h. $DMF{\cdot}SO_3$ was then dropped slowly into the solution within 30 min and the mixture was kept at 50 ^{o}C for 3 h. The solution was then left to cool to RT, and the product was poured into a saturated alkaline ethanolic solution of anhydrous sodium acetate (600 mL). The precipitate that formed was washed with a mixture of ethanol and ddH_2O (ethanol: ddH_2O, 4:1, v:v) and subsequently dissolved in ddH_2O. The pH of the solution was then adjusted to 7.5. The resultant solution was dialyzed against ddH_2O for 48 h using a 10 kDa dialysis cut-off membrane and then lyophilized.

Thiolation of chitosan-arginine: Ch-Arg and sulfated derivatives were modified with single thiol groups at the reducing terminus via reductive amination as previously described [45] to enable analysis of growth factor binding (see section 6.3.1). Briefly, each Ch-Arg preparation was dissolved in ddH_2O and cystamine hydrochloride in MeOH was added to the solution at 500× equiv. Acetic acid was then added to obtain a mixture of MeOH:ddH_2O:acetic acid (35:50:15). The reaction vessel was sealed and brought to 40 °C for 40 min while stirring. The reducing agent, 2-picoline-borane in MeOH (5× equiv), was added and the resulting solution was stirred at 40 °C for a further 40 min. The solution was then dialyzed (10 kDa MWCO) with ddH_2O and lyophilized.

Physical characterization of chitosan-based HS mimetics: Attenuated total reflectance-Fourier transform infra-red spectroscopy (ATR-FTIR, Perkin Elmer Spotlight 400) was used to measure changes in the surface chemical structure of the Ch-Arg following sulfation. Spectra were recorded between 650 and 4000 cm^{-1}.

X-ray photoelectron spectroscopy (XPS) spectra were obtained for Ch-Arg and the sulfated derivatives using a Thermo ESCALAB250i X-ray Photoelectron Spectrometer (XPS) with elemental mapping capability and He UV Source. The degree of sulfation was calculated according to the proportion of sulfur (S%) and nitrogen (N%) in the sample using Equation 1.

Equation $$DS\ (\%) = 100 \times \frac{\frac{S\%}{32.06}}{\frac{N\%}{14.007}}. \quad (1)$$

Nuclear magnetic resonance (2D-NMR) was analyzed using HSQC (^{1}H detected heteronuclear single quantum coherence) on a Bruker Avance III 300 solid state NMR operating at 20 °C with a frequency of 600 MHz and an acquisition time of up to 5.5 s to determine the position of sulfation on the Ch-Arg. The samples were dissolved in D_2O and 16 to 32 scans were obtained.

The charge of Ch-Arg and the sulfated derivatives was determined using Zeta potential (Zetasizer Nano ZS, Malvern). Solutions were prepared in both ddH_2O and phosphate buffered saline (PBS).

Culture of human dermal fibroblasts and keratinocytes: Dermal fibroblasts were isolated from human skin discarded from patients undergoing reconstructive surgery and obtained under ethics approval from Concord Hospital (HREC/14/CRGH/173). Briefly, skin sections were incubated in trypsin (0.125%) at 4 °C to separate the dermis from the epidermis. The epidermis was removed and the dermis was comminuted and collagenase digested (0.05%) for 12 h at 37 °C. Following digestion, the suspension was centrifuged at 400 *g* for 10 min and the cell pellet was resuspended in DMEM supplemented with 10% (v/v) fetal bovine serum (FBS), 1% penicillin/streptomycin (P/S), and L-glutamine (basal medium) and cultured in T-flasks. Medium was refreshed every 3 – 4 days and

conditioned medium was collected for analysis. The immortalized keratinocyte cell line, HaCaT (AddexBio, San Diego), was cultured in basal medium in a humidified incubator (37 °C, 5% CO_2). Cells were passaged at 80% confluence and medium changed every 3 – 4 days and conditioned medium was collected for analysis.

Effect of chitosan-based HS mimetics on cell proliferation: Cells were seeded at 5 × 10^3 cells/well in 96 well plates in basal medium and incubated for 24 h at 37◦C. The basal medium was then removed and replaced with either basal medium alone or supplemented with 10 μg mL^{-1} Ch-Arg or sulfated derivatives. Concentration was chosen placed on previously obtained results.[31] Relative cell number was determined after 24, 48 and 72 h using the MTS cell assay (Promega) according to the manufacturer's instructions. Results are presented relative to the number of cells exposed to basal medium.

Isolation of proteoglycans from conditioned medium: Proteoglycans were isolated from the conditioned medium by anion exchange chromatography using a diethylaminoethyl column (DEAE-Sepharose Fast Flow, GE Healthcare) attached to a FPLC system (Biorad). Briefly, the DEAE column was equilibrated at 1 mL/min with running buffer (250 mM NaCl, 20 mM Tris, 10 mM EDTA, pH 7.5) before the addition of conditioned medium and base-line absorbance was re-established with running buffer. Proteoglycans were eluted from the column using 1 M NaCl, 20 mM Tris, 10 mM EDTA, pH 7.5 and concentrated.

Characterization of proteoglycans: Proteoglycans produced by the dermal fibroblasts and keratinocytes were analyzed by mass spectrometry following enrichment as described in section 6.5.1. For analysis, samples were reduced (10 mM dithiothreitol for 10 min at 95 °C), alkylated (25 mM iodoacetamide for 20 min at 25 °C), and digested with trypsin (sequencing grade; Promega, Sydney, Australia) in 50 mM NH_4HCO_3 at 30 °C for 16 h. Samples were prepared at a final concentration of 500 µg/mL and a final volume of 20 µL. Samples were analyzed by liquid chromatography coupled to tandem mass spectrometry (LC-MS^2) using an LTQ mass spectrometer (Thermo Fisher Scientific). The results were analyzed with Xcalibur™ software (Bioworks version 3.1, Thermo Fisher Scientific) and the Mascot database (Matrix Science, London, UK; version 2.5.1) with a National Centre for Biotechnology Information (NCBI) protein (*Homo sapiens*) database.

Enzyme linked immunosorbent assay (ELISA) was used to confirm that the dermal fibroblasts and keratinocytes produced both perlecan and HS. High binding 96-well ELISA plates (Greiner, Australia) were coated with proteoglycan-enriched fractions of conditioned medium from keratinocytes and fibroblasts (10 µg mL^{-1}) at 37 °C for 16 h. Samples analyzed for the presence of HS stubs were incubated with 0.01 U mL^{-1} heparinase III (h'ase III) at 37 °C for 16 h prior to coating ELISA wells. Wells were rinsed twice with PBS followed by blocking with 0.1% (w/v) casein in PBS for 1 h at 25 °C. Wells were then rinsed twice with PBS with 1% (v/v) Tween 20 (PBST) followed by incubation with primary antibodies diluted in 0.1% (w/v) casein in PBS for 2 h at RT. Primary antibodies included rabbit polyclonal anti-perlecan (1:1000, raised in house against immunopurified endothelial perlecan [35]) and mouse monoclonal anti-HS stub antibody (1 µg/mL, clone 3G10, US Biological). Wells were rinsed twice with PBST followed by incubation with biotinylated secondary antibodies, anti-mouse IgG, or anti-rabbit (1:1000, GE Healthcare) for 1 h at RT, rinsed twice with PBST, and

incubated with streptavidin horseradish peroxidase (1:500, GE Healthcare) for 30 min at RT. Wells were then rinsed four times with PBST, followed by the addition of the colorimetric substrate, 2 mM 2,2-azinodi-3-ethylbenzthiazoline sulfonic acid in 0.5 M sodium citrate, pH 4.6, and absorbance was measured at 405 nm.

Western blotting was used to confirm the production of perlecan by dermal fibroblasts and keratinocytes. Proteoglycan-enriched fractions of conditioned medium from keratinocytes and fibroblasts (3 µg/lane) were electrophoresed in 3–8% (w/v) Tris-Acetate gels (Invitrogen) under reducing conditions (0.1M dithiolthreitol) using Tris-acetate buffer (50 mM tricine, 50 mM Tris, 0.1% (w/v) SDS, pH 8.24) at 160 V for 45 min. Some samples were incubated with 0.01 U/mL h'ase III at 37 °C for 16 h prior to electrophoresis. A series of molecular mass markers (Himark, Invitrogen) were electrophoresed on each gel. Samples were then transferred to polyvinylidene difluoride (PVDF) membrane using transfer buffer (5 mM Bicine, 5 mM BisTris, 0.2 mM EDTA, 50 µg/ml SDS, 1% (v/v) methanol, pH 7.2) in a semidry blotter at 300mA and 20 V for 60 min. The membrane was blocked with 1% (w/v) bovine serum albumin (BSA) in Tris-buffered saline (TBS) (20mM Tris base, 136mM NaCl, pH 7.6) with 0.1% (v/v) Tween 20 (TBST) for 2 h at 25 °C followed by incubation with mouse monoclonal anti-perlecan antibody (2 µg/mL, clone 5D7-2E4, Merck) diluted in 1% (w/v) BSA in TBST for 16 h at 4 °C. Membranes were subsequently rinsed with TBST, incubated with secondary HRP-conjugated antibodies (1:50,000, Invitrogen) for 45 min at 25 °C, and rinsed with TBST and TBS before being imaged using chemiluminescence reagent (Femto reagent kit, Pierce) and x-ray film.

Effect of chitosan-based HS mimetics on HSPG2 gene expression: Keratinocytes and dermal fibroblast cells were cultured in basal medium alone or supplemented with 10 µg/mL Ch-Arg or sulfated derivatives for either 4 or 24 h. Total RNA was isolated with TRI reagent (1 mL per $10^6 - 10^7$ cells) and treated with DNase using the RQ1 RNase-Free DNase kit (Promega). RNA (1µg) was transcribed into cDNA using oligo d(T)23 primer mix (ProScript® M-MuLV First Strand cDNA synthesis kit, GeneSearch). For quantitative real-time PCR (qPCR), 1µL cDNA was mixed with 0.5 µl of 10 µM forward (5'-GGTGCCAGAGCGGGTG-3') and reverse (5'- GCCCTGGAACTTGCCCTG-3') *HSPG2* primers and 10 µL Power SYBR Green PCR Master Mix (Applied Biosystems, Mulgrave, Australia) and 9.5 µL RNAase free water. GAPDH (forward primer 5'-AGAAGGCTGGGGCTCATTTG-3' and reverse primer 5'-AGGGGCCATCCACAGTCTTC-3') was used as an endogenous control and to normalize the results. Samples were subject to 40 reactions using the ABI StepOne™ Real-time PCR system.

Growth factor interactions with chitosan-based HS mimetics: Growth factor, FGF2 and FGF7, binding to Ch-Arg and the sulfated derivatives was evaluated using surface plasmon resonance (BIAcore 2000, GE) operated with PBS, pH 7.4 as the buffer. Thiolated derivatives of the materials were used for analysis as the unthiolated materials did not immobilize with high enough density to the gold sensor chips to enable analysis (Supplementary Figure 1A). Thiolated derivatives were immobilized to the gold sensor chips at a flow rate of 5 µL/min to obtain a minimum of 1000 response units (RU) which was sufficient to form a monolayer on the surface of the sensor chips. To minimize the level of non-specific binding of the growth factors, the surface of the sensor chips were then blocked with 0.1% (w/v) bovine serum albumin (BSA) at a flow rate of 5 µL/min for 5 min. Then either FGF2 (50, 100 or 200 nM, Invitrogen) or FGF7 (200 nM, Invitrogen) was applied at a flow rate of 20 µL/min for 1 min and the response was monitored for a further 4 min. Any remaining growth factor was

removed with 1M NaCl at a flow rate of 20 µL/min for 30 s. The level of growth factor binding to Ch-Arg and the sulfated derivatives was compared with the level of binding to immunopurified endothelial perlecan that is decorated exclusively with HS [46] and known to bind each of these growth factors [10, 34]. The binding of these growth factors to perlecan was also analyzed in the absence of its HS that was removed with h'ase III.

Effect of chitosan-based HS mimetics on keratinocyte migration: A 'scratch assay' was used to monitor keratinocyte migration as a simplified model of wound healing. Keratinocytes (2.8×10^3 cells, HaCaT) were seeded into each side of the migration chamber (Ibidi) in basal medium and allowed to adhere for 12 h. The basal medium was removed and cells were placed in serum free medium for 4 h. Following serum starvation, the migration chambers were removed, and cells were exposed to serum free medium alone, supplemented with 10 µg/mL Ch-Arg, sulfated derivatives, heparin (porcine intestinal mucosa), or an FGF2 function blocking antibody (Abcam, clone MC-GF1, 1 µg/mL). Images (3 per well) were captured at 24 h intervals over 72 h and cell migration was determined by measuring the area between the two migrating cell fronts using Image J. The area was determined manually and presented as a percentage of the initial area.

Effect of chitosan-based HS mimetics on skin wound healing in an organotypic skin model: Human dermal fibroblasts (1.5×10^5 cells/mL, passage 3) were suspended in bovine collagen (3 mg/mL, Invitrogen) prepared in basal medium. The suspension was placed in transwells and allowed to gel at 37 °C for 30 min. Basal medium was then added to immerse the gels and incubated for a further 24 h. The medium was then removed and the surface of the fibroblast/collagen gels were coated with

50 µg/mL fibronectin. Human keratinocytes isolated from human skin were used to form the epidermal component of the skin model. Following removal of the epidermis from the dermis as described in 2.3, cells were gently scraped off the newly exposed epidermal and dermal surfaces. Cells were collected, resuspended in keratinocyte growth medium (Lonza) and cultured on ECM coated (Life Technologies) tissue culture polystyrene until 80% confluency was reached. Keratinocytes (passage 1) were seeded onto the surface of each gel (1×10^5/gel) and allowed to adhere before immersion in basal medium supplemented with 50 µg/mL ascorbic acid. Following incubation for 7 days the gels were brought to the air liquid interface for a further 9 days and the samples were cultured for a further 21 days exposed to basal medium alone or supplemented with 10 µg/mL Ch-Arg or sulfated derivatives.

Histological analysis of the organotypic skin model: Organotypic skin samples were fixed in 4% paraformaldehyde for 16 h at 4 °C, dehydrated and embedded in paraffin. Samples were sectioned (4 – 5 µm) and histological characterization was carried out as previously described.[47] Briefly, sections were rehydrated with xylene to remove paraffin and then immersed in a series of ethanol solutions and finally water. Following rehydration, slides were stained with Harris hematoxylin (Fronine, Australia) for 10 min, followed by eosin (Fronine, Australia) for 5 min, before dehydrating and mounting.

For immunohistochemistry, antigen epitope retrieval was performed by immersing the slides after rehydration in 0.01 M sodium citrate (pH 6), followed by heat treatment in a decloaking chamber (Applied Medical, Santa Margarita, CA) at 120 °C for 4 min. The slides were then rinsed with deionized water followed by blocking of endogenous peroxidase with 3% (v/v) H_2O_2 for 5 min. Some slides were also treated with 0.01 U mL^{-1} h'ase III in PBS (pH 7) for 3 h at 37°C. for analysis of HS

expression. The slides were washed with 50 mM Tris-HCl, 0.15 M NaCl, 0.05% (w/v) Tween-20, pH 7.6 (TBST), and then blocked with 1% (w/v) BSA in TBST for 1 h at RT. The slides were incubated with primary antibodies diluted in 1% w/v BSA in TBST at 4°C for 16 h. Primary antibodies included rabbit polyclonal anti-laminin (1:100, Rockland), rabbit polyclonal anti-collagen IV (1:500, Abcam), rabbit polyclonal anti-perlecan (1:100), mouse monoclonal anti-syndecan-1 (2.5 μg mL^{-1}, Abcam), rabbit polyclonal anti-syndecan-4 (1:500, Abcam) and mouse monoclonal anti-HS stub (5 μg mL^{-1}, clone 3G10, US Biological) antibodies. Slides were then washed twice with TBST before incubation with the appropriate biotinylated secondary antibodies (1:500; GE Healthcare) for 1 h at RT. Slides were washed twice with TBST, incubated for 30 min with SA-HRP (1:250; GE Healthcare), rinsed four times with TBST, and then processed for color development with NovaRED chromogen stain (Vector Laboratories; Burlingame CA). The slides were then counterstained with hematoxylin (Gill's #3, Vector Laboratories) for 6 s and rinsed with deionized water. Slides were dehydrated through a graded ethanol series, mounted and imaged using an Aperio XT slide scanner. Slides were also probed with mouse IgG and IgM whole antibodies (5 μg/ml; Invitrogen, Carlsbad, CA) as isotype controls, as well as blocking solution in place of primary antibodies. These conditions did not show positive staining (data not shown), indicating that non-specific binding of primary antibodies or biotinylated secondary antibodies did not occur.

Statistical Analysis: A two-way analysis of variance (ANOVA) was performed to compare multiple conditions while a student's t test (two samples, two tailed distribution assuming equal variance) was used to compare statistical significance between two conditions. Results of $p<0.05$ were considered significant. Experiments were performed in triplicate and carried out three times.

Acknowledgements

This work was supported by funding from the Australian Research Council under the Linkage Project (LP100100504) scheme. The authors also acknowledge the UNSW Mark Wainwright Analytical Centre for assistance with NMR and XPS analyses. Ch-Arg is a proprietary molecule covered by patents US 8,119,780, US 8,658,775, AU 2007257436 and AU 20133211460.

Received: ((will be filled in by the editorial staff))
Revised: ((will be filled in by the editorial staff))
Published online: ((will be filled in by the editorial staff))

References

[1] S. Werner, R. Grose, *Physiol Rev* **2003**, 83, 835.

[2] M. A. Seeger, A. S. Paller, *Adv Wound Care* **2014**, 4, 213.

[3] A. Yayon, M. Klagsbrun, J. D. Esko, P. Leder, D. M. Ornitz, *Cell* **1991**, 64, 841; I. Capila, R. J. Linhardt, *Angew Chem Int Ed* **2002**, 41, 390; O. Saksela, D. Moscatelli, A. Sommer, D. B. Rifkin, *J Cell Biol* **1988**, 107, 743.

[4] J. D. Esko, S. B. Selleck, *Annu Rev Biochem* **2002**, 71, 435.

[5] K. Lee, E. A. Silva, D. J. Mooney, *J R Soc Interface* **2011**, 8, 153.

[6] S. O. Kolset, G. Pejler, *J Immunol* **2011**, 187, 4927.

[7] Z. Shriver, I. Capila, G. Venkataraman, R. Sasisekharan, *Handb Exp Pharmacol* **2012**, 159.

[8] D. J. Langeslay, C. N. Beecher, A. Naggi, M. Guerrini, G. Torri, C. K. Larive, *Anal Chem* **2013**, 85, 1247.

[9] J. E. Turnbull, D. G. Fernig, Y. Ke, M. C. Wilkinson, J. T. Gallagher, *J Biol Chem* **1992**, 267, 10337.

[10] S. Knox, C. Merry, S. Stringer, J. Melrose, J. Whitelock, *J Biol Chem* **2002**, 277, 14657.

[11] M. W. Tsang, W. K. R. Wong, C. S. Hung, K.-M. Lai, W. Tang, E. Y. N. Cheung, G. Kam, L. Leung, C. W. Chan, C. M. Chu, E. K. H. Lam, *Diabetes Care* **2003**, 26, 1856.

[12] P. W. Finch, J. S. Rubin, T. Miki, D. Ron, S. A. Aaronson, *Science* **1989**, 245, 752.

[13] H. Kaneko, T. Arakawa, H. Mano, T. Kaneda, A. Ogasawara, M. Nakagawa, Y. Toyama, Y. Yabe, M. Kumegawa, Y. Hakeda, *Bone* **2000**, 27, 479; J.-L. Richard, C. Parer-Richard, J.-P. Daures, S. Clouet, D. Vannereau, J. Bringer, M. Rodier, C. Jacob, M. Comte-Bardonnet, *Diabetes Care* **1995**, 18, 64.

[14] B. Farrugia, M. Lord, J. Melrose, J. Whitelock, *Molecules* **2015**, 20, 4254.

[15] H. A. Orgueira, A. Bartolozzi, P. Schell, R. E. J. N. Litjens, E. R. Palmacci, P. H. Seeberger, *Chem Eur J* **2003**, 9, 140; J. L. de Paz, M. Martín-Lomas, *European J Org Chem* **2005**, 2005, 1849; C. L. Cole, S. U. Hansen, M. Baráth, G. Rushton, J. M. Gardiner, E. Avizienyte, G. C. Jayson, *PLoS ONE* **2010**, 5, e11644.

[16] J. Liu, R. J. Linhardt, *Nat Prod Rep* **2014**, 31, 1676.

[17] A. E. Pusateri, S. J. McCarthy, K. W. Gregory, R. A. Harris, L. Cardenas, A. T. McManus, C. W. Goodwin Jr, *J Trauma* **2003**, 54, 177.

[18] I. Y. Kim, S. J. Seo, H. S. Moon, M. K. Yoo, I. Y. Park, B. C. Kim, C. S. Cho, *Biotechnol Adv* **2008**, 26, 1; T. Dai, M. Tanaka, Y. Y. Huang, M. R. Hamblin, *Expert Rev Anti Infect Ther* **2011**, 9, 857; S. Y. Ong, J. Wu, S. M. Moochhala, M. H. Tan, J. Lu, *Biomaterials* **2008**, 29, 4323.

[19] G. Vikhoreva, G. Bannikova, P. Stolbushkina, A. Panov, N. Drozd, V. Makarov, V. Varlamov, L. Gal'braikh, *Carbohydr Polym* **2005**, 62, 327.

[20] J. Yang, K. Luo, D. Li, S. Yu, J. Cai, L. Chen, Y. Du, *Int J Biol Macromol* **2013**, 52, 25.

[21] Y.-C. Ho, S.-J. Wu, F.-L. Mi, Y.-L. Chiu, S.-H. Yu, N. Panda, H.-W. Sung, *Bioconjug Chem* **2009**, 21, 28; H.-Y. Zeng, Y.-C. Huang, *J Polym Res* **2018**, 25, 83.

[22] Y. Yu, J. Chen, R. Chen, L. Cao, W. Tang, D. Lin, J. Wang, C. Liu, *ACS Appl Mater Interfaces* **2015**, 7, 9982; Y. Yu, R. Chen, Y. Sun, Y. Pan, W. Tang, S. Zhang, L. Cao, Y. Yuan, J. Wang, C. Liu, *Acta Biomater* **2018**, 71, 510.

[23] X. Peng, Y. Yu, Z. Wang, X. Zhang, J. Wang, C. Liu, *RSC Adv* **2017**, 7, 43161.

[24] L. Cao, Y. Yu, J. Wang, J. A. Werkmeister, K. M. McLean, C. Liu, *Mater Sci Eng C* **2017**, 74, 298; D. Peschel, K. Zhang, S. Fischer, T. Groth, *Acta Biomater* **2012**, 8, 183; L. Cao, J. Wang, J. Hou, W.

Xing, C. Liu, *Biomaterials* **2014**, 35, 684; Y. Pan, J. Chen, Y. Yu, K. Dai, J. Wang, C. Liu, *Biomater Sci* **2018**, 6, 431.

[25] H. Zhou, J. Qian, J. Wang, W. Yao, C. Liu, J. Chen, X. Cao, *Biomaterials* **2009**, 30, 1715.

[26] H. Tang, P. Zhang, T. L. Kieft, S. J. Ryan, S. M. Baker, W. P. Wiesmann, S. Rogelj, *Acta Biomater* **2010**, 6, 2562.

[27] R. A. Lahmer, A. P. Williams, S. Townsend, S. Baker, D. L. Jones, *Food Control* **2012**, 26, 206.

[28] B. Xiao, Y. Wan, M. Zhao, Y. Liu, S. Zhang, *Carbohydr Polym* **2011**, 83, 144.

[29] V. M. Gaspar, J. G. Marques, F. Sousa, R. O. Louro, J. A. Queiroz, I. J. Correia, *Nanotechnology* **2013**, 24, 275101.

[30] Y. Gao, Z. Xu, S. Chen, W. Gu, L. Chen, Y. Li, *Int J Pharm* **2008**, 359, 241; D. Oh, A. Nasrolahi Shirazi, K. Northup, B. Sullivan, R. K. Tiwari, M. Bisoffi, K. Parang, *Mol Pharm* **2014**, 11, 2845; H.-X. Lv, Z.-H. Zhang, X.-P. Wang, Q.-Q. Cheng, W. Wang, X.-H. Huang, J.-P. Zhou, Q. Zhang, L.-L. Hou, W. Huo, *Molecules* **2011**, 16, 6778.

[31] M. Lord, B. M. Tsoi, B. L. Farrugia, S. R. S. Ting, S. Baker, W. P. Wiesmann, J. Whitelock, *J Mater Chem B* **2014**, 2, 6517.

[32] B. P. Antunes, A. F. Moreira, V. M. Gaspar, I. J. Correia, *Carbohydr Polym* **2015**, 130, 104.

[33] Y. R. Hsu, R. Nybo, J. K. Sullivan, V. Costigan, C. S. Spahr, C. Wong, M. Jones, A. G. Pentzer, J. A. Crouse, R. E. Pacifici, H. S. Lu, C. F. Morris, J. S. Philo, *Biochemistry* **1999**, 38, 2523.

[34] M. Mongiat, K. Taylor, J. Otto, S. Aho, J. Uitto, J. M. Whitelock, R. V. Iozzo, *J Biol Chem* **2000**, 275, 7095.

[35] M. S. Lord, C. Y. Chuang, J. Melrose, M. J. Davies, R. V. Iozzo, J. M. Whitelock, *Matrix Biol* **2014**, 35, 112.

[36] R. Xing, S. Liu, H. Yu, Z. Guo, Z. Li, P. Li, *Carbohydr Polym* **2005**, 61, 148; K. Zhang, J. Helm, D. Peschel, M. Gruner, T. Groth, S. Fischer, *Polymer* **2010**, 51, 4698.

[37] M. S. Lord, A. L. Ellis, B. L. Farrugia, J. M. Whitelock, H. Grenett, C. Li, R. L. O'Grady, A. A. DeCarlo, *J Control Release* **2017**, 250, 48.

[38] B. Goger, Y. Halden, A. Rek, R. Mösl, D. Pye, J. Gallagher, A. J. Kungl, *Biochemistry* **2002**, 41, 1640; K. M. Poluri, P. R. B. Joseph, K. V. Sawant, K. Rajarathnam, *J Biol Chem* **2013**, 288, 25143; M. A. Seeger, A. S. Paller, *Adv Wound Care* **2015**, 4, 213.

[39] S. Ye, Y. Luo, W. Lu, R. B. Jones, R. J. Linhardt, I. Capila, T. Toida, M. Kan, H. Pelletier, W. L. McKeehan, *Biochemistry* **2001**, 40, 14429.

[40] I. Sher, S. Zisman-Rozen, L. Eliahu, J. M. Whitelock, N. Maas-Szabowski, Y. Yamada, D. Breitkreutz, N. E. Fusenig, E. Arikawa-Hirasawa, R. V. Iozzo, R. Bergman, D. Ron, *J Biol Chem* **2006**, 281, 5178.

[41] Z. Zhou, J. Wang, R. Cao, H. Morita, R. Soininen, K. M. Chan, B. Liu, Y. Cao, K. Tryggvason, *Cancer Res* **2004**, 64, 4699.

[42] M. A. Stepp, H. E. Gibson, P. H. Gala, D. D. S. Iglesia, A. Pajoohesh-Ganji, S. Pal-Ghosh, M. Brown, C. Aquino, A. M. Schwartz, O. Goldberger, M. T. Hinkes, M. Bernfield, *J Cell Sci* **2002**, 115, 4517.

[43] K. Elenius, S. Vainio, M. Laato, M. Salmivirta, I. Thesleff, M. Jalkanen, *J Cell Biol* **1991**, 114, 585.

[44] F. Echtermeyer, M. Streit, S. Wilcox-Adelman, S. Saoncella, F. Denhez, M. Detmar, P. F. Goetinck, *J Clin Invest* **2001**, 107, R9.

[45] I. Unterieser, P. Mischnick, *Carbohydr Res* **2011**, 346, 68; R. I. W. Osmond, W. C. Kett, S. E. Skett, D. R. Coombe, *Anal Biochem* **2002**, 310, 199.

[46] J. M. Whitelock, L. D. Graham, J. Melrose, A. D. Murdoch, R. V. Iozzo, P. Anne Underwood, *Matrix Biol* **1999**, 18, 163.

[47] B. L. Farrugia, J. M. Whitelock, M. Jung, B. McGrath, R. L. O'Grady, S. J. McCarthy, M. S. Lord, *Biomaterials* **2014**, 35, 1462.

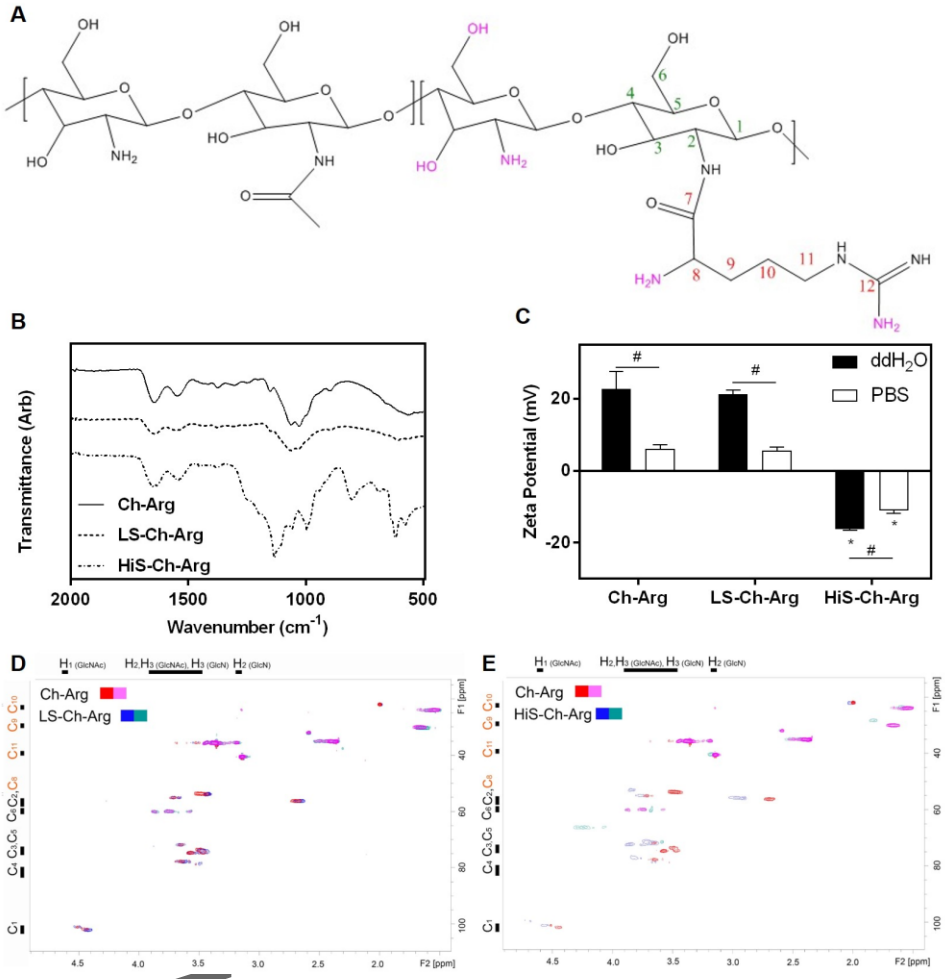

Figure 1. Characterization of chitosan-based HS mimetics. (A) Schematic of Ch-Arg indicating possible sites of sulfate incorporation (pink) at carbon positions on the chitosan backbone (C_1-C_6; green) and arginine side chain (C_8-C_{12}; red). (B) ATR-FTIR spectra and (C) zeta-potential of Ch-Arg, LS-Ch-Arg and HiS-Ch-Arg. Data presented as mean ± standard deviation (n=3). # indicates significant difference for each material between ddH_2O and PBS (p<0.05). * indicates significant difference in zeta potential compared to Ch-Arg (p<0.05). HSQC spectra of (D) Ch-Arg and LS-Ch-Arg and (E) Ch-Arg and HiS-Ch-Arg.

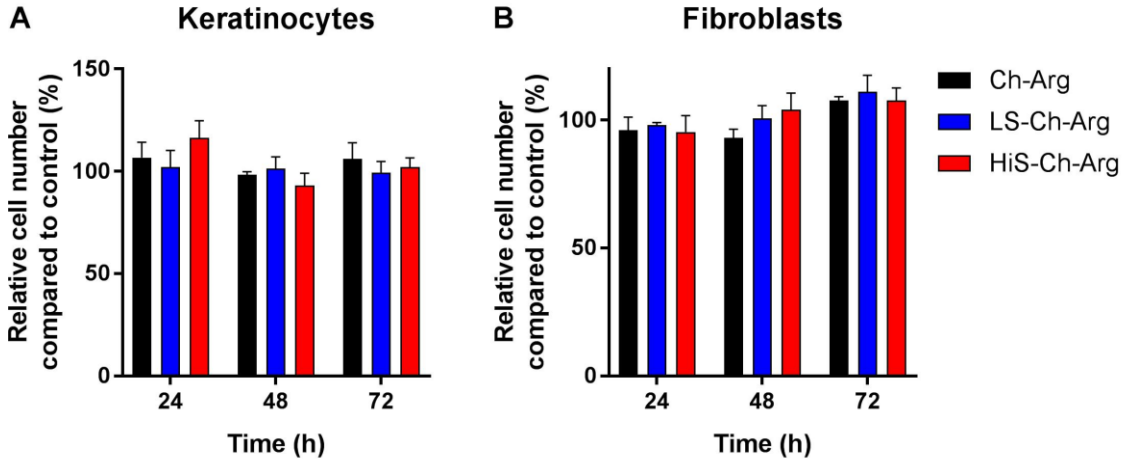

Figure 2. **Ch-Arg and the sulfated derivatives are not cytotoxic**. Relative number of (A) keratinocytes and (B) fibroblasts measured over a period of 72 h exposed to Ch-Arg or sulfated derivatives at a concentration of 10 µg/mL compared to cells exposed to basal medium (control), as measured by the MTS assay. Data presented at mean ± standard deviation (n = 3).

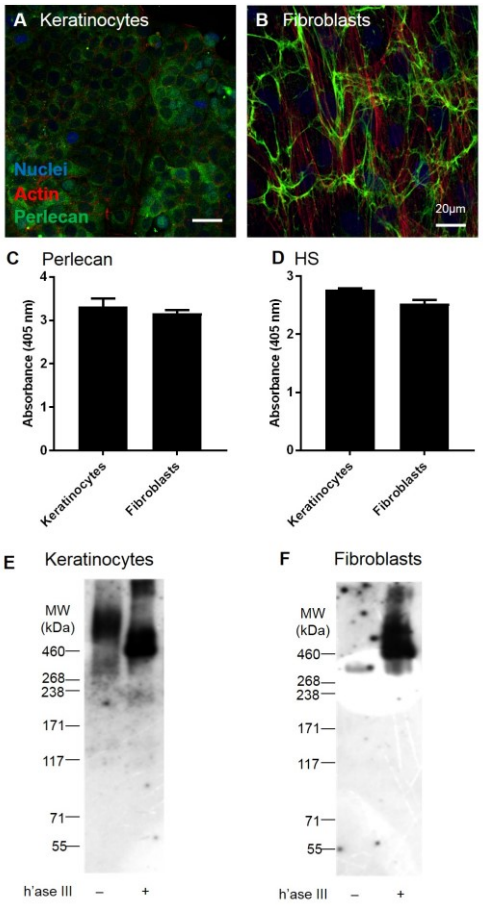

Figure 3. Keratinocytes and fibroblasts produce perlecan and HS. Expression of perlecan (green) by (A) keratinocytes and (B) fibroblasts determined by immunocytochemistry and counterstained for actin cytoskeleton (red) and nuclei (blue). Scale bar indicates 20 µm. Detection of (C) perlecan (polyclonal antibody CCN-1) and (D) HS (antibody clone 3G10 detects the HS stub following h'ase III digestion) in conditioned medium from cultures of keratinocytes and fibroblasts. Data presented at mean ± standard deviation (n = 3). Western blot analysis of perlecan produced by (E) keratinocytes and (F) fibroblasts detected by antibody clone 5D7-2E4. Samples were analyzed undigested or digested with h'ase III.

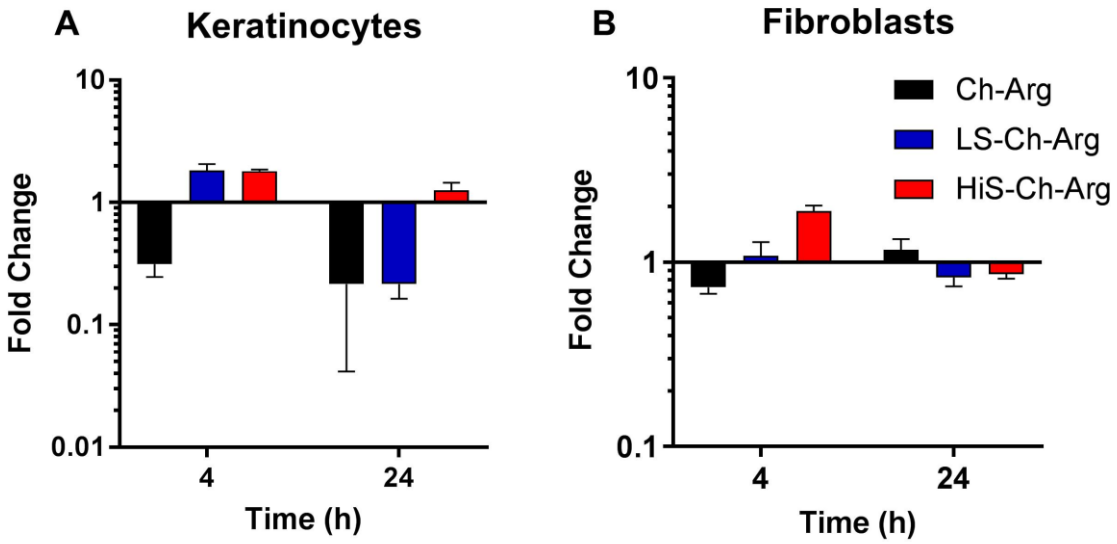

Figure 4. Sulfated Ch-Arg promotes early *HSPG2* gene expression. Quantitative PCR analysis of *HSPG2* gene expression by (A) keratinocytes and (B) fibroblasts exposed to basal medium alone or supplemented with Ch-Arg, LS-Ch-Arg or HiS-Ch-Arg (10 µg mL^{-1}) for up to 24 h. Data presented a fold change in *HSPG2* gene expression compared to cells exposed to basal medium and corrected for *GAPDH* expression for each treatment.

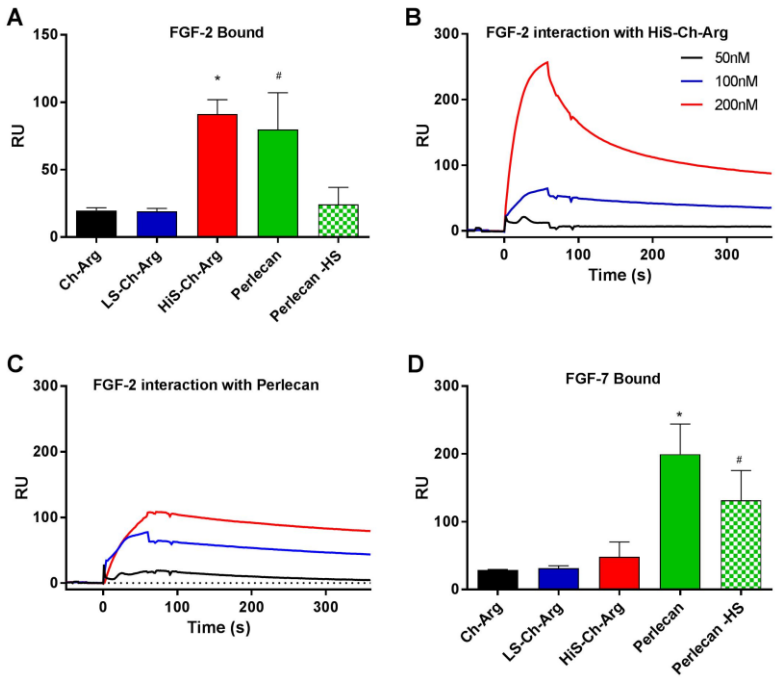

Figure 5. Chitosan-based HS mimetics bind FGF2 with higher affinity than perlecan HS. (A) The level of FGF2 bound to Ch-Arg, LS-Ch-Arg, HiS-Ch-Arg, perlecan or perlecan without HS chains (Perlecan-HS) presented in response units (RU) as measured by surface plasmon resonance. * indicates significant difference to all conditions except perlecan ($p \leq 0.05$). # indicates significant difference to conditions except HiS-Ch-Arg ($p \leq 0.05$). (B) Sensorgrams of FGF2 (50, 100 and 200 nM) binding to (B) HiS-Ch-Arg and (C) perlecan. One representative curve (of triplicates) at each concentration is shown. For kinetic analysis, all curves were utilized for each concentration. (D) The level of FGF7 bound to Ch-Arg, LS-Ch-Arg, HiS-Ch-Arg, perlecan or perlecan without HS chains (perlecan-HS) presented in RU as measured by surface plasmon resonance. * indicates significant difference to all test conditions ($p \leq 0.05$). # indicates significant difference to Ch-Arg and the sulfated derivatives ($p \leq 0.05$).

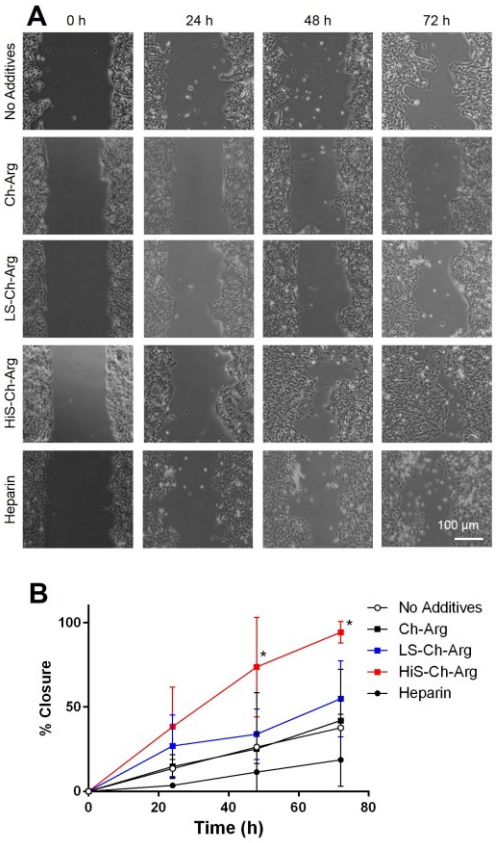

Figure 6. Chitosan-based HS mimetics promote keratinocyte migration. Keratinocyte migration measured in a 'scratch assay' over 72 h for cells exposed to basal medium alone or supplemented with 10 µg/mL Ch-Arg or sulfated derivatives. (A) Sample phase contrast images of the migration zone in each condition at 0, 24, 48 and 72 h. Scale bar indicates 100 µm. (B) Analysis of the phase contrast images was performed by measuring the area between the two migrating cell fronts at each time point and presented as a proportion of the initial area. * indicates significant difference to all other conditions at the same time points (p<0.05).

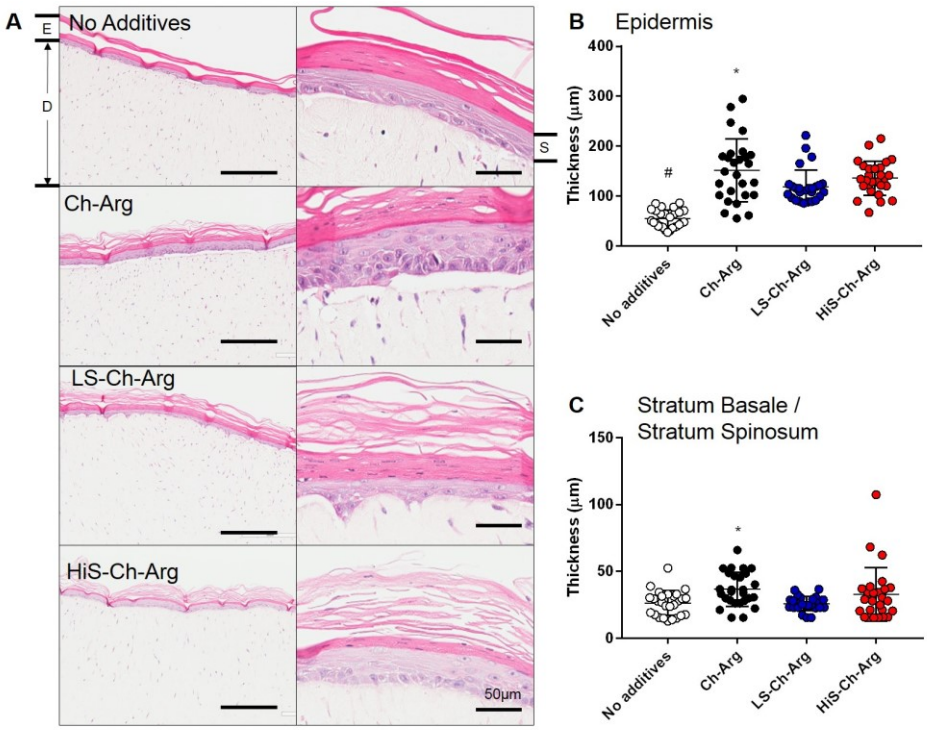

Figure 7. Chitosan-based HS mimetics promote epidermal formation. (A) Representative images of the organotypic skin model indicating the epidermis (E), dermis (D) and stratum basale / stratum spinosum (S) following exposure to basal medium alone or supplemented with Ch-Arg, LS-Ch-Arg or HiS-Ch-Arg. Sections were stained with hematoxylin and eosin. Scale bar represents 50 µm. Quantification of the (B) epidermal and the (C) stratum basale/stratum spinosum thickness in the organotypic skin model following exposure to each of the conditions. In panel B, * indicates significant difference compared to LS-Ch-Arg (p<0.05) and $^{\#}$ indicates significant difference compared to Ch-Arg and the sulfated derivatives (p<0.05). In panel C, * indicates significant difference compared to no additives and Ch-Arg (p<0.05)

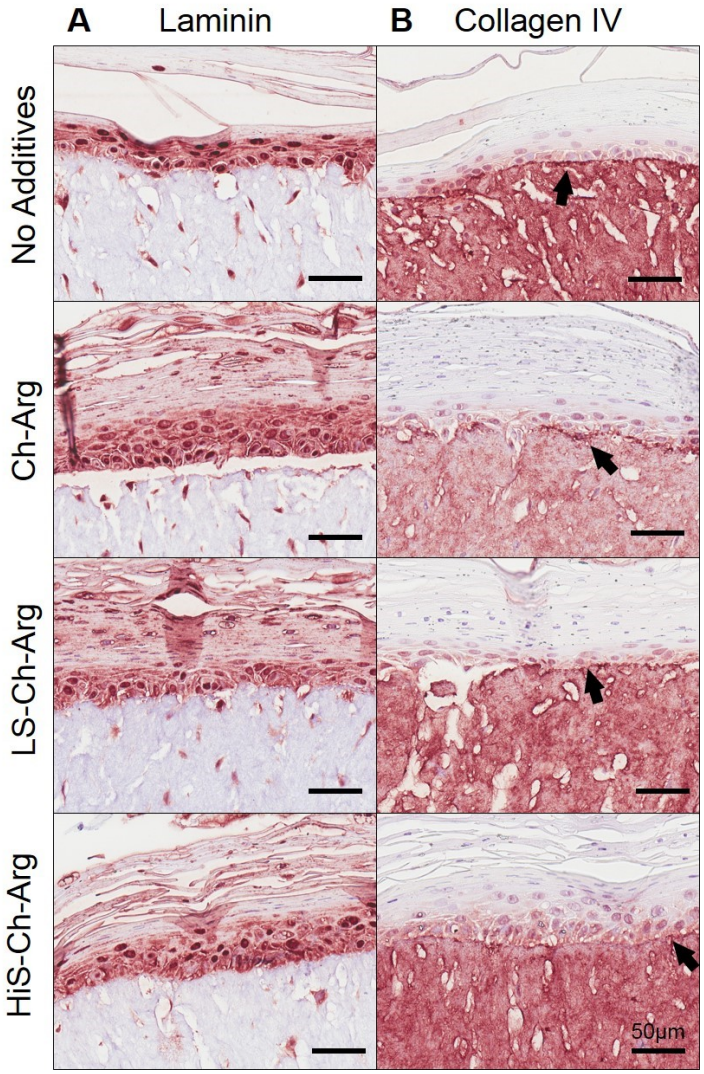

Figure 8. Chitosan-based HS mimetics support the expression of basement membrane components. Expression of (A) laminin and (B) collagen type V in the organotypic skin model following exposure to basal medium alone or supplemented with Ch-Arg, LS-Ch-Arg or HiS-Ch-Arg. Scale bars represent 50 µm.

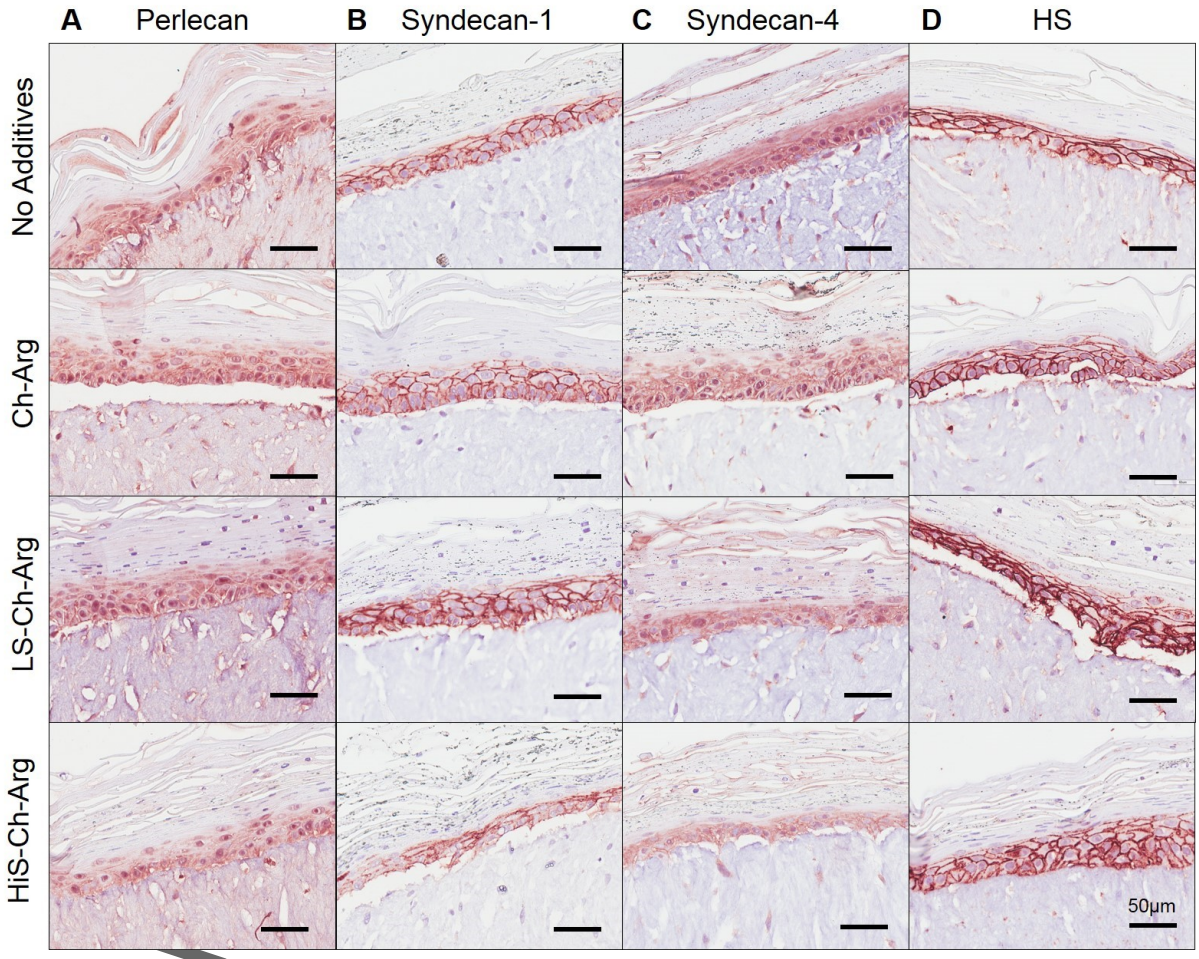

Figure 9. Chitosan-based HS mimetics support the expression of HS proteoglycans. Expression of (A) perlecan, (B) syndecan-1, (C) syndecan-4 and (D) HS in the organotypic skin model following exposure to basal medium alone or supplemented with Ch-Arg, LS-Ch-Arg or HiS-Ch-Arg. Scale bars represent 50 µm.

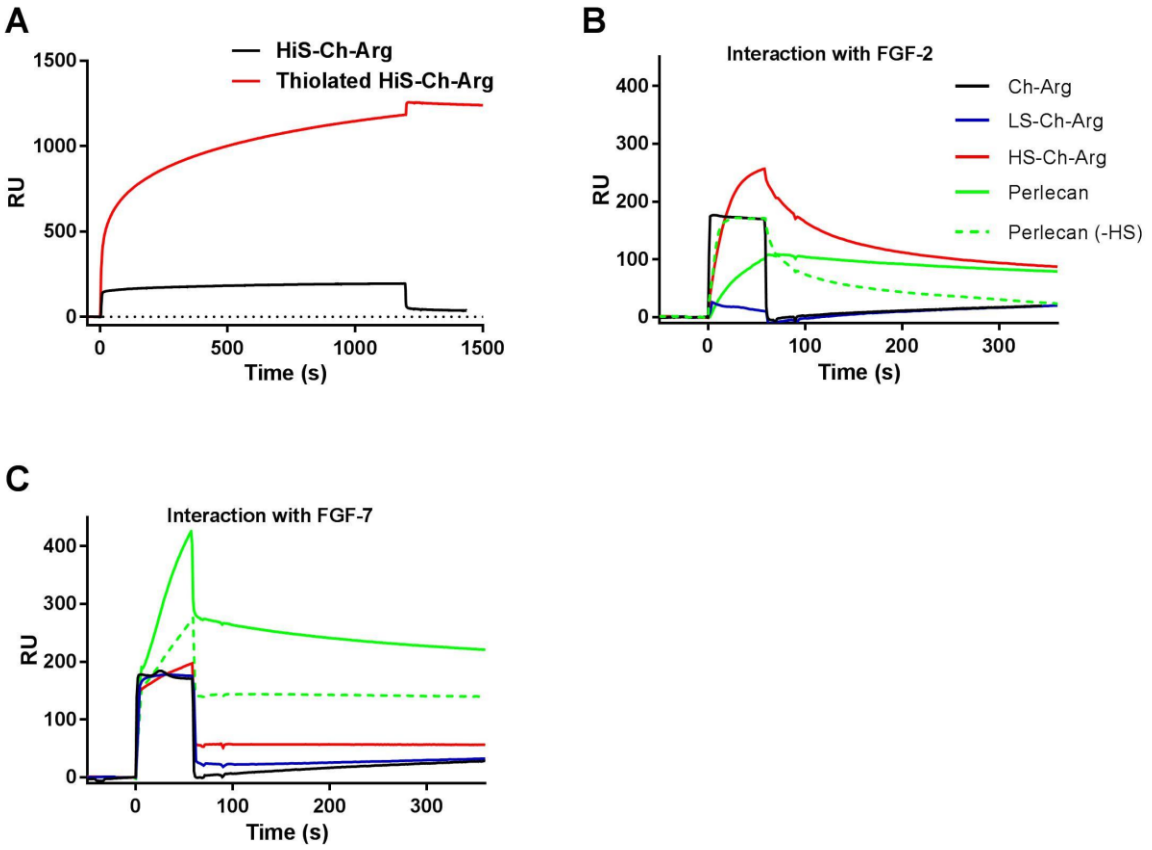

Supplementary Figure 1. Sensorgrams of (A) HiS-Ch-Arg and thiolated HiS-Ch-Arg binding to gold sensor surfaces indicating that only thiolated HiS-Ch-Arg was stably immobilized. (B) FGF2 (200 nm) and (C) FGF7 (200 nM) binding to Ch-Arg, LS-Ch-Arg, HiS-Ch-Arg, perlecan and perlecan without HS (perlecan-HS). One representative curve (of triplicates) at each concentration is shown.

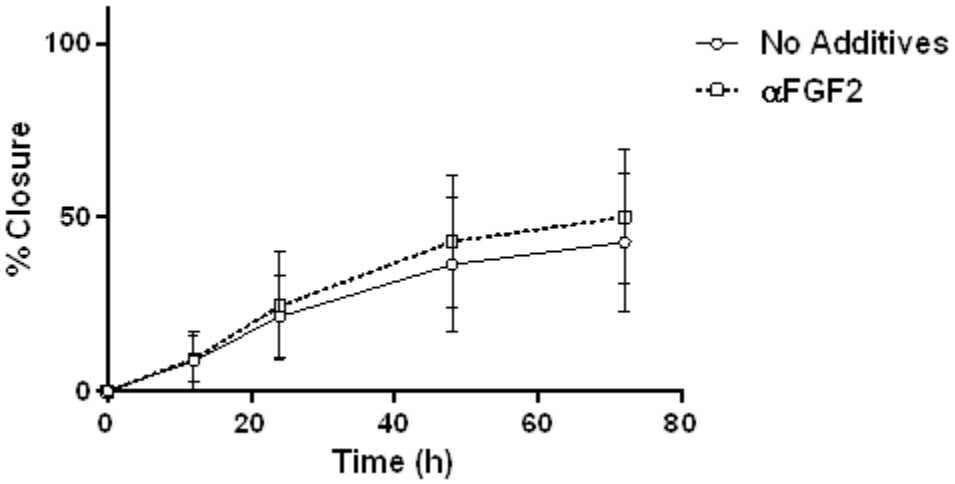

Supplementary Figure 2. Keratinocyte migration measured in a 'scratch assay' over 72 h for cells exposed to basal medium alone or supplemented an anti-FGF2 blocking antibody (α-FGF2).

Table 1. Elemental content of Ch-Arg, LS-Ch-Arg and HiS-Ch-Arg determined by XPS.

	Percent (%)				
	C	**N**	**O**	**S**	**DS**
Ch-Arg	56.15	13.63	28.61	0	0
LS-Ch-Arg	57.47	11.71	29.28	0.78	3
HiS-Ch-Arg	34.76	6.03	41.65	8.04	58

Table 2. HS proteoglycans secreted by keratinocytes and fibroblasts detected by peptide LC-MS[2] from an in-solution tryptic digestion.

	HS proteoglycans	MOWSE score[a]		Accession number[b]
		Keratinocytes	Fibroblasts	
Extracellular	Agrin	1664	51	O00468
	Collagen type XVIII	103	215	P39060
	Perlecan	610	1540	P98160
Cell surface	Glypican	239	76	P35052
	Syndecan-1	63	-	P18827
	Syndecan-4	235	76	P31431

[a] Molecular mass search score as determined by Mascot query. This is the value (p) that is a measure of the probability that the match is a random event expressed as -10log (p). The higher the score, the more confidence that the match is not due to a random event. [b] Obtained from Swiss-Prot. -, not detected.

'Modification of chitosan-arginine to incorporate sulfate groups mimics heparan sulfate (HS), a binding partner of growth factors. By altering the degree of sulfate modification this biomimetic material has the potential to assist in wound healing through the binding of growth factors (GF), promotion of epithelial cell migration and epidermis formation.